Journal of Power Sources 225 (2013) 316–322

Contents lists available at SciVerse ScienceDirect

Journal of Power Sources

journal homepage: www.elsevier.com/locate/jpowsour

Tin and graphite based nanocomposites: Potential anode for sodium ion batteries

Moni Kanchan Datta [a,b], Rigved Epur [c], Partha Saha [a], Karan Kadakia [d], Sung Kyoo Park [a], Prashant N. Kumta [a,b,c,d,e,*]

[a] Bioengineering, Swanson School of Engineering, University of Pittsburgh, PA 15261, USA
[b] Center for Complex Engineered Multifunctional Materials, University of Pittsburgh, PA 15261, USA
[c] Mechanical Engineering and Materials Science, Swanson School of Engineering, University of Pittsburgh, PA 15261, USA
[d] Chemical and Petroleum Engineering, Swanson School of Engineering, University of Pittsburgh, PA 15261, USA
[e] Department of Oral Biology, School of Dental Medicine, University of Pittsburgh, PA 15261, USA

HIGHLIGHTS

- Tin and graphite mixture and nanocomposites have been synthesized by high energy mechanical milling (HEMM).
- Mechanically milling results in nanocrystalline nanocomposites.
- The mechanically milled nanocomposites exhibit stable capacities of ~410 mAh g^{-1}.
- Electrochemical response varies with duration of mechanical milling.
- Good electrochemical response of the nanocomposite is due to structural stability.

GRAPHICAL ABSTRACT

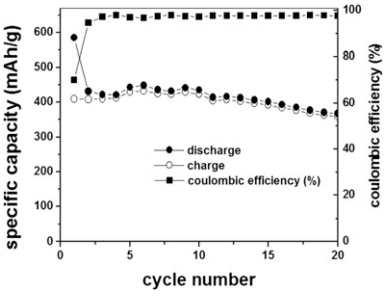

ARTICLE INFO

Article history:
Received 21 August 2012
Received in revised form
4 October 2012
Accepted 8 October 2012
Available online 16 October 2012

Keywords:
Sn/C nanocomposite
Na-ion batteries
Anode
High energy mechanical milling

ABSTRACT

Pure tin (Sn) and a homogeneous nanocomposite of tin and graphite (C), denoted as Sn/C, have been studied as a suitable anode for sodium ion batteries. The Sn/C nanocomposites have been synthesized by high energy mechanical milling (HEMM) of pure Sn and graphite of nominal composition C-70 wt.% Sn. Pure microcrystalline Sn (≤44 μm) exhibits a 1st discharge capacity ~856 mAh g^{-1} which is close to the expected theoretical capacity, however, it shows a large 1st cycle irreversible loss (~67%) and the anticipated inevitable rapid fade in capacity expectedly due to structural failure of the electrode. On the other hand, the resultant Sn/C based nanocomposite, synthesized by HEMM after 1h of milling, exhibits a 1st cycle discharge capacity ~584 mAh g^{-1} with a 1st cycle irreversible loss ~30%. The Sn/C nanocomposite shows a 1st cycle charge capacity of ~410 mAh g^{-1} with improved capacity retention in comparison to pure Sn displaying 0.7% fade in capacity per cycle up to 20 cycles when cycled at a rate of ~C/8. Scanning electron microscopy (SEM) analysis indicates that the structural integrity and microstructural stability of the Sn/C nanocomposite during the alloying/dealloying processes appear to be the primary factors contributing to the good cyclability observed in the above HEMM derived nanocomposite suggesting its promise as a potential anode for Na-ion systems.

1. Introduction

Renewable energy sources such as solar, wind, geothermal and hydropower can generate electricity without producing carbon dioxide, the undesirable green house pollutant. Hence these

* Corresponding author. Bioengineering, Mechanical Engineering and Materials Science, Chemical and Petroleum Engineering Swanson School of Engineering, University of Pittsburgh, PA 15261, USA. Tel.: +1 41 26480223; fax: +1 41 26243699.
E-mail address: pkumta@pitt.edu (P.N. Kumta).

0378-7753/$ – see front matter © 2012 Elsevier B.V. All rights reserved.
http://dx.doi.org/10.1016/j.jpowsour.2012.10.014

systems portend enormous potential for meeting the future energy demands [1–3]. However, the electricity generated from these intermittent renewable sources requires efficient electrical energy storage (EES) devices for effective delivery of uninterrupted electricity (power storage back up) and load leveling as well as grid energy storage [1–4]. In addition, there is a tremendous global impetus for improved EES devices so that smooth transition from the current hybrid electric vehicle state to that of the much touted plug-in hybrids and the highly desired all-electric vehicles (EVs) is ultimately realized [1–4]. Chemical energy storage technologies based on rechargeable batteries are considered one of the leading EES technologies to meet this target offering the much desired panacea for both electric vehicles as well as stand-alone stationary power systems [1–6]. Currently Li-ion batteries are the preferred much sought after rechargeable battery systems for most electronic devices and hybrid cars [1–10]. However, in the last few years, a variety of factors have led to considerable interest in Na-ion batteries employing Na^+ to reversibly store power in a compact system offer a compelling economical solution for electrical energy storage [11–15]. In contrast to the Li-ion system that has been researched extensively over the last two decades following its commercialization by Sony in 1990, Na-ion battery is still in a very much in the developmental research phase. Nevertheless, it has become a target of much debate of late, and is forecasted to be a cheaper (cost equivalent of dollars for bulk metal: Na: 0.075, Li: 0.50), more durable option to store energy compared to the hitherto used Li-ion batteries [11–15]. Moreover, Li is relatively in less abundance (~0.0007% by weight of the earth's crust), whereas Na is much more copiously available (~2.6% by weight of the earth's crust) [11–16]. Na-ion is also chemically more stable compared to Li-ion battery and more environmentally benign. Consequently large-scale Na-ion EES device have the potential to be easier to engineer and pose less safety concerns [11–15,17,18]. If the evolution of Li-ion and Na-ion batteries is assumed to follow a similar trajectory, it is likely that Na-ion batteries will soon emerge an attractive alternative front runner due to the low cost, larger abundance and other environmental combined with socio-economic attributes.

In order for Na-ion to compete with the much researched Li-ion systems, considerable improvement in energy density and rate capability along with performance is required before sodium/liquid organic electrolyte batteries can be considered for practical use as EES devices. Identification of suitable cathodes and anodes which can exhibit high specific capacity, low irreversible loss, high coulombic efficiency and long cycle life as well as can intercalate/de-intercalate Na^+ at potential above ~3 V for cathode and ~0.01–1 V for anode of Na/Na^+ will be a paradigm shift in the development of high energy density Na-ion rechargeable batteries for EES systems. These systems will support rapid transition to EVs as well as wind and solar energy, distributed energy systems, or 'smart' grid operations. In addition, fundamental studies of alloying/dealloying mechanism of Na^+ with metal alloy anodes and ceramic cathodes will provide valuable information for designing new systems. There is therefore a critical need for significant research to be conducted in the Na-ion battery area, particularly related to identification of new materials and chemistries while also developing cost effective approaches to generate these systems to achieve the much desired radical improvements in energy and power densities. Few studies of candidate negative electrodes for Na-ion battery can be found in the current scientific literature [11,19–25]. It is now well known that graphite and silicon though well established in the case of the former and the latter very much researched for Li-ion, however cannot be used as a negative electrode for Na-ion systems since Na atoms do not reversibly alloy/dealloy to form Na–C or Na-Si alloys similar to the Li counterpart (e.g. LiC_6 or $Li_{4.4}Si$, respectively) [24,26]. Recent reports suggest the identification of nanoporous hard carbons as possible negative electrode materials, wherein Na atoms apparently adsorb instead of alloying onto the surfaces or nanoscopic pores throughout the hard carbon particles [19–23]. Doeff et al. [20] showed that insertion of Na into petroleum-coke leads to a reversible capacity ~85 mAh g^{-1} and proved the feasibility of a rechargeable Na-ion battery with the selection of appropriate electrode materials. Several researchers [19–23] have studied the electrochemical absorption of Na into some hard carbon structures and found that a reversible capacity ~250–300 mAh g^{-1} could be achieved. Such carbons appear to be suitable anodic materials for rechargeable Na-ion batteries, however, deposited Na metal on C surfaces or nanopores appears to form dendrites similar to Li and its safety is further questionable due to its low melting point of 97.7 °C compared to 180.5 °C for Li. Chevrier and Ceder [24] recently examined theoretically the viability of Na-ion negative electrode materials based on Na alloys (Na–Si, Na–Sn and Na–Pb system) in terms of volumetric energy density and mechanical stability. They have reported the formation of different Na–Sn alloys ($NaSn_5$, NaSn, Na_9Sn_4 and $Na_{15}Sn_4$) in the potential window of 0–0.7 V associated with large volume expansion. The calculated volume expansion of different Na–Sn alloys with respect to Sn along with the theoretical specific capacity (mAh g^{-1}) associated with the formation of the respective phases is tabulated in Table 1. It should be noted that although these Na–Sn phases appear to be similar to Li–Sn Zintl type phases, it is not clear at present if all of the Na–Sn phases exhibit characteristics of an intermetallic or Zintl type phase. Hence both terminologies have been used to indicate all of the alloys in the Na–Sn system. Komaba et al. [25] has reported a 1st cycle discharge and 1st cycle charge capacity ~878 mAh g^{-1} and ~758 mAh g^{-1}, respectively, of Sn-polyacrylic acid electrode with rapid fade in capacity when cycled in the potential window 0–1.5 V. On the other hand, SnSb/C nanocomposite has been reported to exhibit a reversible capacity ~540 mAh g^{-1} with 80% capacity retention after 50 cycles [11]. In spite of the above reports, Na–Sn alloys as negative electrodes have yet to be extensively studied experimentally in order to improve the long-term cyclability, coulombic efficiency and specific capacity for future applications in EES devices. In the present study, a homogeneous mixture based on tin and graphite (Sn/C) has been studied as a negative electrode for Na-ion batteries. To demonstrate efficacy, Sn/C nanocomposite have been prepared by high-energy mechanical milling (HEMM) for different duration of milling. In order to compare the electrochemical results of Sn/C with pure microcrystalline Sn, the electrochemical properties of pure microcrystalline Sn alone has also been studied. Results of these preliminary studies have been documented in the present manuscript indicating feasibility of this system as a potential anode for use in Na batteries.

2. Experimental details

Mixtures of elemental powders of synthetic graphite (Aldrich, 1–2 μm) and Sn (Alfa Aesar, −325 mesh, ≤44 μm) of nominal

Table 1
Intermetallic sodium stannide (Zintl phases) with their molar volume (V_m) and the volume expansion $(V_m - V_{Sn})/V_{Sn}$ per mole of Sn with the theoretical capacity (mAh g^{-1}) associated with the formation of respective phases by alloying of sodium with tin.

Intermetallics	V_m (cm^3 mol^{-1})	$(V_m - V_{Sn})/V_{Sn}$ (%)	Gravimetric capacity (mAh g^{-1})
$NaSn_5$	~21.0	~28%	~45
NaSn	~35.8	~120	~226
Na_9Sn_4	~56.74	~248	~508
$Na_{15}Sn_4$	~85.40	~424	~847

V_{sn} is the molar volume of Sn (~16.30 cm^3 mol^{-1}).

composition C-70 wt.% Sn were subjected to high energy mechanical milling (HEMM) in a high energy shaker mill (SPEX CeriPrep 8000M) for 5 min and 1 h in a stainless steel (SS) vial using 20 SS balls of 2 mm diameter (~20 g) with a ball to powder weight ratio of 10:1. Graphite (~0.6 g) and Sn (~1.4 g) were batched in a SS vial in an argon filled glove box (MBraun Unilab Work station(1200/780)) in order to prevent oxidation of the reactive powders during milling.

In order to perform qualitative phase analysis, the milled powders were characterized by X-ray diffraction (XRD) using the Philips PW1830 system employing the CuK_α ($\lambda = 0.15406$ nm) radiation. The microstructure the electrode before and after electrochemical cycling has been carried out using a scanning electron microscope (SEM) equipped with energy dispersive x-ray analysis (EDAX). Philips XL-30FEG equipped with an EDS detector system comprised of an ultrathin beryllium window and Si(Li) detector operating at 25 kV was employed for the secondary electron (SE) image. Micro-Raman analyses of the Sn/C mixture and nanocomposite have been performed on a multichannel Renishaw InVia Raman microscope. Excitation was provided by the ~633 nm line of a diode laser.

In order to evaluate the electrochemical characteristics, electrodes were fabricated by mixing 80 wt.% of the active powder of −325 mesh and 10 wt.% Super P carbon black. A solution containing 10 wt.% polyvinylidene fluoride (PVDF) in *N*-methyl-pyrrolidinone was added to the mixture to make a homogeneous solution. The as prepared solution was coated onto a Cu foil and dried at 110 °C in a vacuum oven. A 2016 coin cell design was used employing sodium foil as the counter electrode, electrodes comprising materials currently under study as the working electrode and 1 M $NaClO_4$ in ethylene carbonate/dimethyl carbonate (EC/DMC = 1:2 in volume) as the electrolyte. All the cells tested in this study were cycled at room temperature (~298 K) within 0.01–1.2 V employing the discharge/charge rates of ~50 mA g^{-1} with a minute rest period between the charge/discharge cycles using a multichannel battery testing system (Arbin BT2000 instrument).

3. Results and discussion

Fig. 1 shows the variation of specific capacity vs. cycle number of pure microcrystalline Sn (≤44 μm) cycled at a rate of ~50 mA g^{-1} in the potential window 0.01–1.2 V. As shown in Fig. 1, pure Sn shows a 1st discharge capacity ~856 mAh g^{-1} which is close to the theoretical capacity (~847 mAh g^{-1}) corresponding to the formation of $Na_{15}Sn_4$ intermetallic or amorphous phase of composition Na-21at.% Sn (see Table 1). The observed 1st discharge capacity in the present study is also in good agreement with the previous reports [11,25]. The differential capacity plot (d*Q*/d*V* vs. *V*) relating to the 1st cycle of pure Sn, shown in Fig. 2, clearly shows that the alloying reaction (discharge) of Na ion with microcrystalline Sn occurs mainly at a peak potential of ~0.18 V, ~0.081 V and ~0.033 V with an onset potential of ~0.21 V, ~0.13 V and ~0.063 V, respectively. In the present study, the phase/es forming corresponding to the peak potential of ~0.18 V, ~0.081 V and ~0.033 V has been denoted as X-I, X-II and X-III, respectively. The reaction potential and the associated specific capacity, calculated from the deconvolution of the peaks, related to X-I, X-II and X-III phase formation is tabulated in Table 2. The composition of the X-I, X-II and X-III phases, estimated based on the associated specific capacity of the respective phases related to the number of reacting sodium ions, is correspondingly close to Na-50at.% Sn (NaSn), Na-30.7% Sn (Na_9Sn_4) and Na-21at.% Sn ($Na_{15}Sn_4$), respectively. However, pure Sn shows a 1st charge capacity of ~280 mAh g^{-1} with an irreversible loss of ~67% (Fig. 1) which is expected to arise due to the structural failure of Sn particles and/or irreversible alloying/dealloying processes of Sn with Na very similar to what is known in Li alloying with Si [7,26]. The differential capacity plot of 1st charge, shown in Fig. 2, show that the dealloying reaction (charge) of Na ion from X-III phase occurs only at a peak potential of ~0.17 V with an onset potential of ~0.065 V which suggest that the alloying and dealloying reaction of pure microcrystalline Sn with Na ion is irreversible in nature. The differential capacity plot of 2nd cycle of pure Sn, shown in Fig. 3, shows that the formation of X-I and X-II phase observed during the 1st discharge (Fig. 2) is bypassed in the 2nd cycle. The detailed phase formation and transformation during electrochemical alloying/dealloying processes of Na ion with Sn is currently under investigation and will be published very shortly. The SEM images of pure microcrystalline

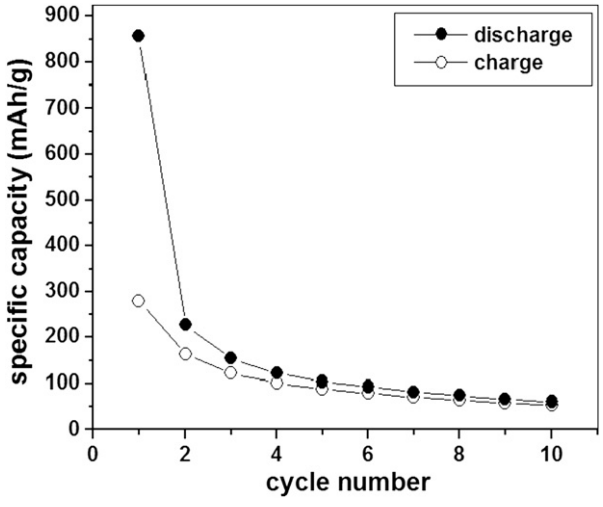

Fig. 1. Specific capacity vs. cycle number of pure microcrystalline Sn (≤44 μm) cycled at a constant current of ~50 mA g^{-1} in the potential window 0.01–1.2 V.

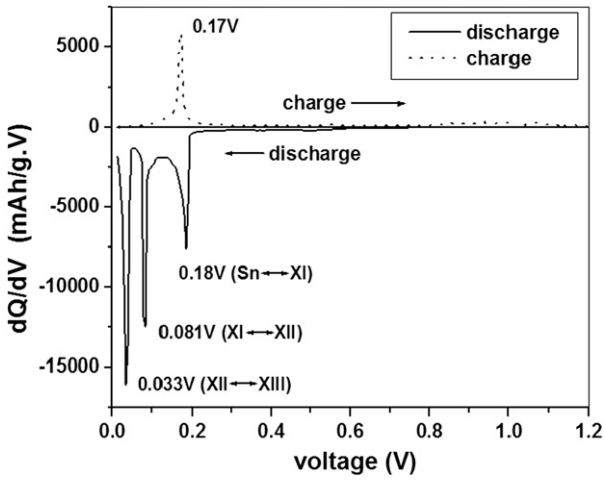

Fig. 2. Differential capacity vs. cell potential curves of pure microcrystalline Sn obtained after 1st cycle cycled at ~50 mA g^{-1} in the potential window 0.01–1.2 V.

Table 2
Reaction potential (V) and associated specific capacity (mAh g^{-1}) of different intermetallics (Zintl phases) form during alloying of Na ion with pure Sn.

Reaction potential window (V)	Peak potential (V)	Associated specific capacity (mAh g^{-1})	Intermetallic
~0.21–0.13	~0.18	~215	X-I (NaSn)
~0.13–~0.063	~0.081	~260	X-II (Na_9Sn_4)
~0.063V-0.01V	~0.033	~325	X-III ($Na_{15}Sn_4$)

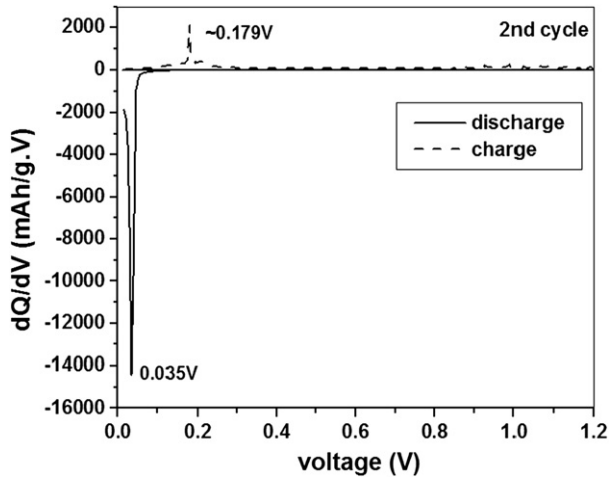

Fig. 3. Differential capacity *vs.* cell potential curves of pure microcrystalline Sn obtained after 2nd cycle cycled at ~50 mA g^{-1} in the potential window 0.01–1.2 V.

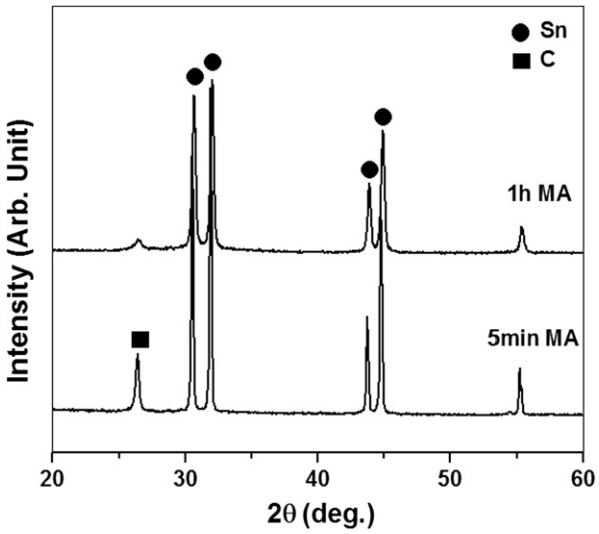

Fig. 5. XRD patterns of C-70 wt.% Sn homogeneous mixture generated after 5 min and 1 h of milling.

Sn before cycling and after the 10th cycle, shown in Fig. 4a, b, respectively, shows clear evidence of structural failure of the cycled Sn. The mechanical failure of pure Sn during the alloying/dealloying processes is expected to arise due to the large volume expansion (~420%) occurring during alloying of Sn with Na to form $Na_{15}Sn_4$ (Table 1), and as a result, loss of electrical contact between the cracked and isolated Sn particles, and the current collector as is evident in the case of elemental Si when cycled with Li^+ [7,26].

In order to improve the structural integrity and cyclability of Sn based anode, a homogeneous mixture based on Sn and graphite has been synthesized by high energy mechanical milling milled for different duration. The mechanical properties, and as a result the-structural stability of Sn/C nanocomposite is expected to be improved due to the presence of graphitic buffer matrix. After 5 min and 1 h of mechanical milling of Sn and graphite of nominal composition C-70 wt.% Sn, the XRD pattern, shown in Fig. 5, shows only the presence of pure Sn and graphite without the formation of any second phase or oxidation of Sn to SnO_2. This result clearly suggests that graphite and Sn form a homogeneous mixture up to 1 h of milling without any significant diffusive reaction to form a second phase as also expected from the equilibrium phase diagram which shows immiscibility of Sn and C due to the positive heat of reaction [27]. The effective crystallite size of Sn obtained after 1 h of milling, calculated using the Scherrer formula from the integral breadth of the Lorentzian contribution determined from the peak profile analysis using single line approximation method after eliminating the instrumental broadening and lattice strain contribution [28,29], is ~90 nm, whereas the crystallite size of Sn after 5 min of milling is still in the micron range suggesting that HEMM for 1 h results in the formation of a nanocomposite of Sn and C. On the other hand, the calculated crystallite size of graphite after 5 min and 1 h of milling is ~47 nm and ~17 nm, respectively. In order to investigate the structural order/disorder nature of graphite and the possible presence of SnO_2, Raman spectroscopy analysis of Sn/C obtained after 1 h of milling has been carried out. The Raman spectra of Sn/C, displayed in Fig. 6 along with pure graphite, show peaks at ~1580 cm^{-1} and ~1334 cm^{-1} which corresponds to ordered graphite (G band) and the disordered carbon (D band) [30]. The intensity of D band of disordered carbon appears to increase in the Sn/C nanocomposite in comparison to graphite which clearly suggests that the crystalline graphite structure collapses to form an amorphous disordered form due to the defect induced melting of

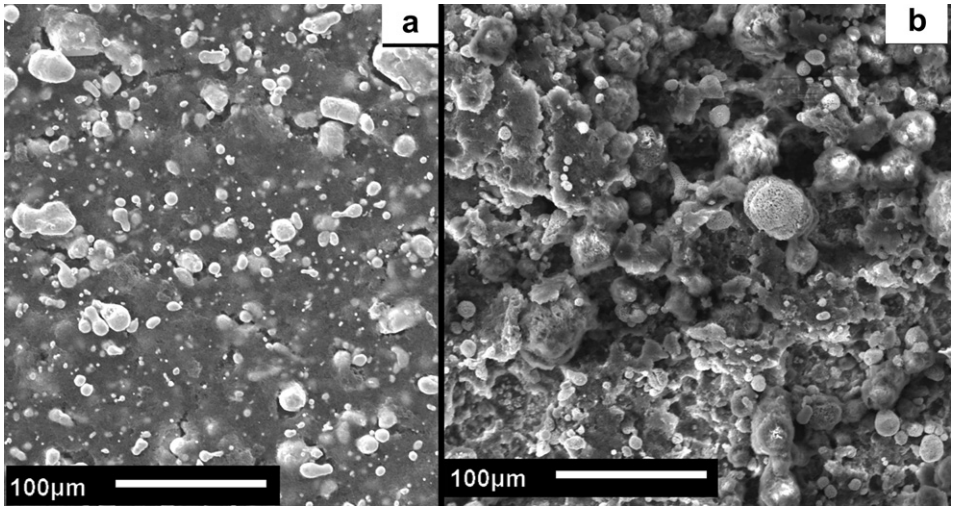

Fig. 4. SEM secondary electron image of pure Sn (a) before and (b) after 10th cycle.

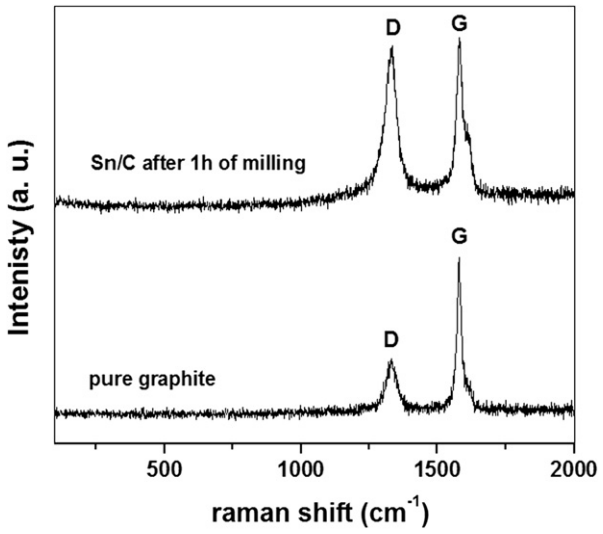

Fig. 6. Raman spectra of Sn/C mixture obtained after 1 h of mechanical milling.

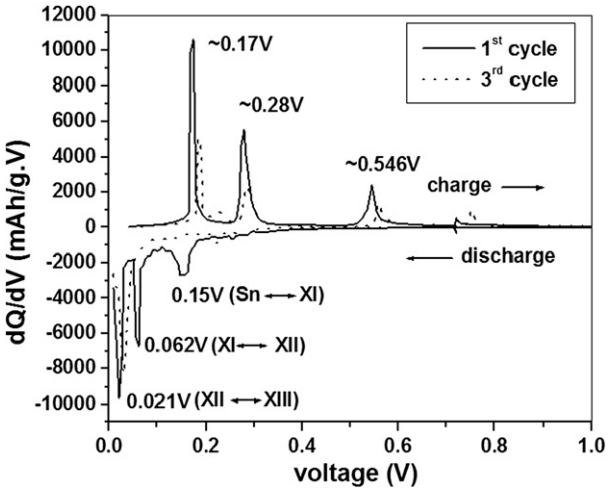

Fig. 8. Differential capacity *vs.* cell potential curves of Sn/C after 5 min of milling obtained after 1st and 3rd cycles cycled at ~50 mA g^{-1} in the potential window 0.01–1.2 V.

crystalline graphite which is commonly observed during HEMM [29,31]. No significant peaks of crystalline SnO_2, normally seen as characteristic sharp peaks at ~474 cm^{-1}, ~632 cm^{-1}, ~774 cm^{-1} corresponding to the E_g, A_{1g} and B_{2g} vibration modes [32] are observed which suggests no oxidation of Sn to SnO_2 during the milling process.

Fig. 7 shows the variation of specific capacity *vs.* cycle number along with coulombic efficiency of the Sn/C mixture synthesized after 5 min of milling, cycled at a constant current of ~50 mA g^{-1} in the potential window 0.01–1.2 V. As shown in Fig. 7, the 1st discharge and 1st charge capacity of the Sn/C mixture obtained after 5 min of milling is ~621 mAh g^{-1} and ~462 mAh g^{-1}, respectively, with a 1st cycle irreversible loss of ~25% and the coulombic efficiency in excess of ~97% after the 1st cycle. This result clearly suggests that the presence of graphite as a matrix in the Sn/C mixture improves the structural stability of Sn/C in comparison to pure Sn during the alloying/dealloying processes with Na. However, a rapid fade in capacity (3.6% per cycle) is observed (Fig. 7) which suggests that HEMM of Sn and C for 5min is not sufficient to generate a strong interfacial bonding in order to improve the mechanical properties and structural integrity of Sn/C for long cycle life. The differential capacity plot (dQ/dV vs. V) relating to the 1st cycle and 3rd cycle of Sn/C mixture obtained after 5 min of milling, shown in Fig. 8, clearly indicates that the alloying reaction (1st discharge) of Na ion with Sn/C occurs mainly at a peak potential of ~0.15 V, ~0.062 V and ~0.021 V which is similar to pure microcrystalline Sn (Table 2). However, the differential capacity plot of 1st and 3rd charging processes, shown in Fig. 8, indicates that the dealloying reaction (charge) of Na ion from X-III phase occurs at peak potentials of ~0.17 V, ~0.28 V and ~0.55 V whereas the desodiation of pure microcrystalline Sn occurs only at ~0.17 V (Fig. 2). This result clearly suggests that the alloying and dealloying reaction of Sn/C with Na is reversible in nature. Furthermore, these results suggest that the milling reaction of Sn with C probably alters the surface and bulk structure of Sn.

On the other hand, the nanocrystalline Sn/C nanocomposite mixture obtained after 1 h of milling shows a 1st discharge and a 1st charge capacity of ~584 mAh g^{-1} and ~410 mAh g^{-1}, respectively, with an irreversible loss of ~29% (Fig. 9) and coulombic efficiency above 97% after the 1st cycle when cycled at an identical current of 50 mA g^{-1} in the potential window 0.01–1.2 V. The 1st cycle irreversible loss may arise due to the electrolyte decomposition at the electrode surface resulting in the formation of a solid electrolyte interphase (SEI) layer and is not

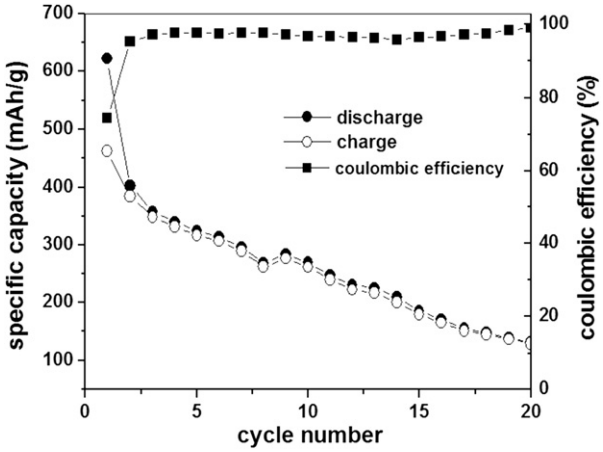

Fig. 7. Specific capacity and coulombic efficiency vs. cycle number of Sn/C obtained after 5 min of milling cycled at a constant current of ~50 mA g^{-1} in the potential window 0.01–1.2 V.

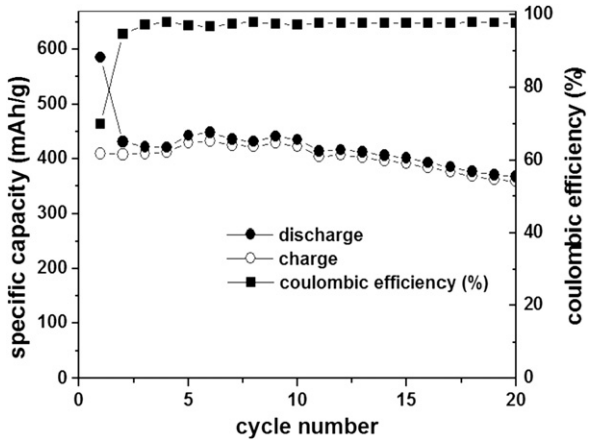

Fig. 9. Specific capacity and coulombic efficiency vs. cycle number of Sn/C obtained after 1 h of milling cycled at a constant current of ~50 mA g^{-1} in the potential window 0.01–1.2 V.

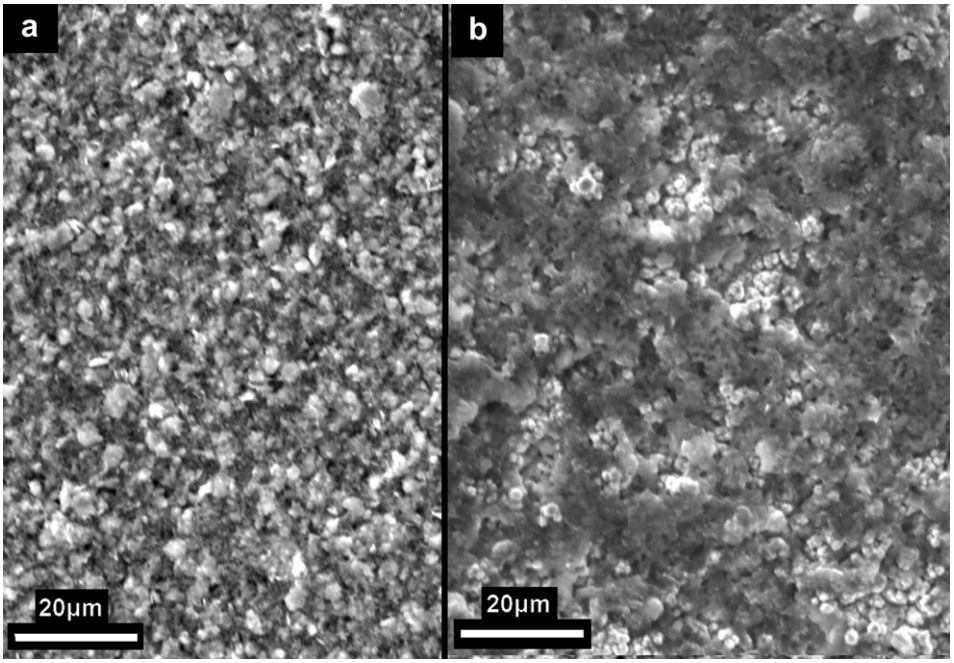

Fig. 10. SEM micrograph of Sn/C mixture, obtained after 1 h of HEMM, before and after 20 cycles.

indicative of an irreversible nature of the Na–Sn/C reaction. However, a detailed study needs to be performed to understand the actual mechanisms involved in the formation of the SEI and the influence of Na^+ on the formation of the SEI. In comparison to pure Sn and the Sn/C mixture obtained after 5 min of milling, the Sn/C nanocomposite obtained after 1 h of milling shows improvement in cyclability up to 20 cycles with a fade in capacity of ~0.7% loss per cycle. This improvement in the cyclability of Sn/C mixture with increasing milling time is expected due to the likely improvement in the mechanical properties of the Sn/C mixture arising from the better interface adhesion and/or bonding between the Sn and C with increasing milling time which is expected to relieve the stress/strain experienced by Sn to the C buffer layer during the alloying/dealloying reaction with sodium ion. The improvement in cyclability also may arise due to the nanocrystalline nature of Sn (~90 nm) and graphite which is known to exhibit better

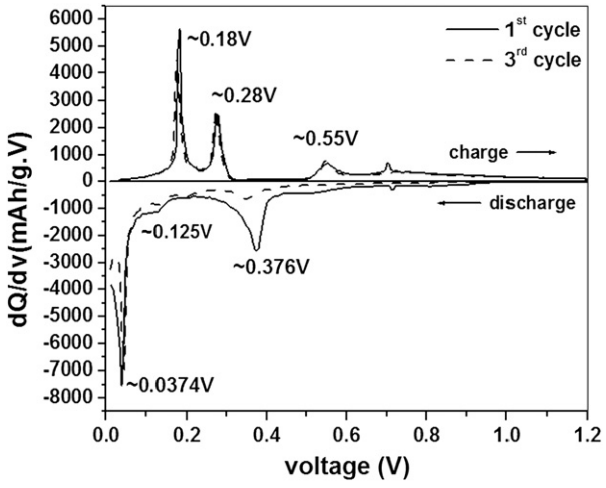

Fig. 11. Differential capacity vs. cell potential curves of Sn/C nanocomposite derived after the 1 h of milling obtained after 1st cycle and third cycle cycled at ~C/8 rate in the potential window 0.01–1.2 V.

mechanical properties in comparison to the Sn and C counterparts in the coarser grained bulk structures. The SEM micrograph of the Sn/C electrode samples cycled at ~50 mA g^{-1}, shown in Fig. 10, indicates the excellent structural integrity (devoid of any cracks) of the electrode even after 20 cycles. The differential capacity plot (dQ/dV vs. V) relating to the 1st cycle and 3rd cycle of nanocrystalline Sn/C composite obtained after 1 h of milling cycled at ~50 mA g^{-1} is shown in Fig. 11. It is clearly evident from Fig. 11 that the alloying reaction (discharge) of Na ion with nanocrystalline Sn/C obtained after 1 h of milling occurs mainly at a peak potential of ~0.376 V and ~0.0374 V which suggest that the alloying reaction of nanocrystalline Sn/C obtained after 1 h of milling is thus different in comparison to pure microcrystalline Sn and Sn/C obtained after 5 min of milling, whereas the dealloying reaction is quite similar to Sn/C obtained after 5 min of milling. The alloying/dealloying mechanism and the effect of alloying/dealloying process on the structural stability of nanocryalline Sn/C is currently under investigation which will be published very shortly. Nevertheless, the above preliminary results clearly suggest that the presence of graphite as a buffer matrix significantly improves the structural stability of the Sn/C with respect to pure Sn. This promising result is a reflection of the much research that is warranted in regards to synthesizing nanocomposites exhibiting high strength, high ductility and strong interface of Sn with the matrix. The result also suggests the need for the identification of suitable binders in order to improve the cyclability, rate capability and coulombic efficiency of Sn based electrodes for use as anodes in sodium ion batteries.

4. Conclusion

In recent years, sodium ion batteries have received extensive interest as electrical energy storage devices due to its more abundance, projected economic benefits, higher safety, and the possible engineering ease in comparison to the hitherto used Li-ion batteries. However, significant research is needed to be performed to identify improved anode and cathode materials for Na-ion batteries which will exhibit high specific capacity, low 1st

cycle irreversible loss, excellent coulombic efficiency and cyclability. In this regard, the present study has been devoted to identify a suitable negative electrode for Na-ion batteries based on a homogeneous mixture of nanocrystalline tin and graphite (Sn/C). Nanocrystalline Sn/C nanocomposite of nominal composition C-70 wt.% Sn has been synthesized by high energy mechanical milling (HEMM) of pure microcrystalline Sn and graphite. Pure microcryalline Sn exhibits a 1st discharge capacity ~856 mAh g^{-1} due to the extensive electrochemical reaction of Na ion with Sn in the peak potential of ~0.18 V, ~0.08 V and ~0.033 V. The phase/s forming corresponding to the peak potential ~0.18 V, ~0.08 V and ~0.033 V, determined from the associated specific capacity, is expected to be NaSn, Na_9Sn_4 and $Na_{15}Sn_4$. However, pure microcrystalline Sn shows a rapid fade in capacity and poor capacity retention due to the large volume expansion of Sn to form $Na_{15}Sn_4$ (~400%). On the other hand, nanocrystalline Sn/C nanocomposite with a crystallite size of Sn ~90 nm shows a 1st discharge and 1st charge capacity ~584 mAh g^{-1} and ~410 mAh g^{-1}, respectively. The nanocrystalline Sn/C mixture generated also shows improved capacity retention (0.7% fade in capacity per cycle) with respect to pure Sn indicating its promise as an anode for Na-ion batteries. Scanning electron microscopy (SEM) analysis indicates that the structural integrity combined with microstructural stability of the Sn/C nanocomposite during the alloying/dealloying process with sodium appear to be the main reasons contributing to the good cyclability in comparison to pure Sn. This buffering capacity of graphite is expected to minimize the volume expansion related cracking of tin enabling its use as anode for sodium ion batteries.

Acknowledgements

The authors gratefully acknowledge the financial support of the DOE-BATT program (contract DE-AC02-05CHl1231), the National Science Foundation (NSF-CBET-0933141) and partial support of the Ford Foundation. The authors also acknowledge the Edward R. Weidlein Chair Professorship funds and the Center for Complex Engineered Multifunctional Materials (CCEMM), University of Pittsburgh for partial support of this research.

References

[1] Basic Research Needs for Electrical Energy Storage, Office of Basic Energy Science, US Department of Energy, Washington, DC, 2007.
[2] M.S. Whittingham, MRS Bulletin 33 (2008) 411.
[3] H.D. Abruna, Y. Kiya, J.C. Henderson, Physics Today 43 (2008).
[4] C. Liu, F. Li, L.P. Ma, H.M. Cheng, Advanced Materials 22 (2010) E28.
[5] T. Reddy, D. Linden, Linden's Handbook of Batteries, Mcgraw-Hill, 2010.
[6] F. Cheng, J. Liang, Z. Tao, J. Chen, Advanced Materials 23 (2011) 1695.
[7] U. Kasavajjula, C. Wang, A.J. Appleby, Journal of Power Sources 163 (2007) 1003.
[8] R. Teki, M.K. Datta, R. Krishnan, T.C. Parker, T.M. Lu, P.N. Kumta, N. Koratkar, Small 5 (2009) 2236.
[9] M.K. Datta, J. Maranchi, S.J. Chung, R. Epur, K. Kadakia, P. Jampani, P.N. Kumta, Electrochimica Acta 56 (2011) 4717.
[10] B. Kang, G. Cedar, Nature 458 (2009) 190.
[11] L. Xiao, Y. Cao, J. Xiao, W. Wang, L. Kovarik, Z. Nie, J. Liu, Chemical Communications 48 (2012) 3321.
[12] S.W. Kim, D.H. Seo, X. Ma, G. Ceder, K. Kang, Advanced Energy Materials 2 (2012) 710.
[13] N. Yabuuchi, M. Kajiyama, J. Ieatate, H. Nishikawa, S. Hitomi, R. Okuyama, R. Usui, Y. Yamada, S. Komaba, Nature Materials (2012). http://dx.doi.org/10.1038/NMAT3309.
[14] S. Tepavcevic, H. Xiong, V.R. Stamenkovic, X. Zuo, M. Balasubramanian, V.B. Prakapenka, C.S. Johnson, T. Rajh, ACS Nano 6 (2012) 530.
[15] Y. Cao, L. Xiao, W. Wang, D. Choi, Z. Nie, J. Yu, L.V. Saraf, Z. Yang, J. Liu, Advanced Materials 23 (2011) 3155.
[16] David R. Lide (Ed.), CRC Handbook of Chemistry and Physics, Taylor & Francis, 2008.
[17] J.F. Whitacre, A. Tevar, S. Sharma, Electrochemistry Communications 12 (2010) 463.
[18] J.F. Whitacre, T. Wiley, S. Shanbhag, Y. Wenzhuo, A. Mohamed, S.E. Chun, E. Weber, D. Blackwood, E. Lynch-Bell, J. Gulakowski, C. Smith, D. Humphreys, Journal of Power Sources 213 (2012) 255.
[19] S. Komaba, W. Murata, T. Ishikawa, N. Yabuuchi, T. Ozeki, T. Nakayama, A. Ogata, K. Gotoh, K. Fujiwara, Advanced Functional Materials 21 (2011) 3859.
[20] M.M. Doeff, Y. Ma, S.J. Visco, L.C. De Jonghe, Journal of Electrochemical Society 140 (1993) L169.
[21] D.A. Stevens, J.R. Dahn, Journal of Electrochemical Society 148 (2001) A803.
[22] K. Tang, L. Fu, R.J. White, L. Yu, M.M. Titrici, M. Antonietti, J. Maier, Advanced Energy Materials 2 (2012) 873.
[23] X. Xia, J.R. Dahn, Journal of Electrochemical Society 159 (2012) A515.
[24] V.L. Chevrier, G. Ceder, Journal of Electrochemical Society 158 (2011) A1011.
[25] S. Komaba, Y. Matsuura, T. Ishikawa, N. Yabuuchi, W. Murata, S. Kuze, Electrochemical Communications 21 (2012) 65.
[26] M.K. Datta, P.N. Kumta, Journal of Power Sources 194 (2009) 1043.
[27] T.B. Massalski, H. Okamoto, P.R. Subramanian, L. Kacprzak (Eds.), Binary Alloy Phase Diagram, second ed., vol. 1, ASM International, Materials Park, Ohio, 1990.
[28] T.H. de Keijser, J.I. Langford, E.J. Mittemeijer, A.B.P. Vogels, Journal of Applied Crystallography 15 (1982) 308.
[29] M.K. Datta, Synthesis and characterization of Fe-Ni-Si system synthesized by mechanical alloying. Ph.D. thesis, Indian Institute of Technology, Kharagpur, India (2002).
[30] J. Nanda, M.K. Datta, J.T. Remillard, A. O'Neill, P.N. Kumta, Electrochemical Communications 11 (2009) 235.
[31] C. Ettl, K. Samwer, Materials Sciences Engineering A 178 (1994) 245.
[32] S.H. Sun, G.W. Meng, G.X. Zhang, T. Gao, B.Y. Geng, L.D. Zhang, J. Zuo, Chemical Physics Letters 376 (2003) 103.